

# Jet noise due to direct radiation of acoustic waves: shear layer radiation and leaking trapped waves

By S. Görtz<sup>†</sup>, L. De Broeck<sup>†</sup>, O. Martin, M. Oberlack<sup>†‡</sup>, AND S. K. Lele

We investigate continuous outward radiating modes for the model problem of a planar isothermal supersonic jet with constant core flow, constructed from two opposite hyperbolic tangent shear layers. The modes are obtained by means of an analytical solution of the corresponding inviscid eigenvalue problem (EVP) and are validated and extended to a more complete physical model by using the analytical solution as input data for a direct numerical simulation (DNS). We observe two classes of waves, both of which are oscillatory in the field-field of the jet and consequently radiate sound. The first class of modes describes acoustic waves generated in both shear layers of the jet without interaction between the shear layers. They are characterized by having zero amplitude in the core flow and radiating only wavelike in the field-field of the jet. We call them pure shear layer radiating modes. The second class of modes are so-called leaking trapped waves, which represent acoustic waves in the core flow that are partially reflected in the core, resulting in trapped waves, but also partially transmitted through the shear layers. The outward transmitted part of these waves consequently leads to sound radiation.

---

## 1. Introduction

Jet noise poses a considerable challenge in various aerospace engineering applications, particularly in high-speed flight regimes. Reducing jet noise is crucial for minimizing noise while maintaining improved efficiency. Since the pioneering work of Lighthill (1952), therefore, numerous experimental and numerical investigations of the causes and influencing factors of jet noise have been carried out. Nevertheless, noise generation in jets is not yet fully understood. In jets, noise is mainly generated by fine-scale turbulence structures or coherent structures in the form of wave packets. In the subsonic case they are associated with a predominantly evanescent near-field pressure, while for the supersonic case, the wave packets lead to the so-called Mach wave radiation, exceeding the noise generation of the fine-scale structures (Jordan & Colonius 2013). Another cause of noise radiation in supersonic jets is the shock cell structures there, which give rise to screech tones and broadband shock associated noise (Tam 1995).

Of importance for this work is the connection between acoustic wave radiation into the jet's field-field and instability waves within the jet. The idea of linking flow noise to instability waves, representing large-scale structures, is quite natural and may be traced back to the pioneering work of Tam (1971) and the great progress on instabilities in supersonic jets by Tam & Hu (1989). They identified three families of unstable modes for a high-speed jet. Of special interest are those having supersonic phase velocity with respect to the outer flow, since these supersonic modes are able to radiate sound into the field-field. This was first shown by Tam & Burton (1984) using the method of matched

<sup>†</sup> Graduate School of Computational Engineering, TU Darmstadt, Germany

<sup>‡</sup> Chair of Fluid Dynamics, TU Darmstadt, Germany

asymptotic expansions, where the unstable mode, decaying in the outer limit of the flow, is matched at the edge of the shear layer with a purely oscillatory solution, representing the sound wave radiated to the field-field. This method has since then been variously extended by the Wu group, who also accounted for the role of nonlinearities in the process of radiation (Wu & Zhang 2019). The theoretical results on the Mach wave radiation of supersonic modes were first confirmed for an axisymmetric supersonic jet in a DNS by Mitchell *et al.* (1997). Considering the radiating modes, which are supersonic with respect to the outer flow, a further classification can be made for the considered jet with core flow. If the modes are also supersonic with respect to the core flow, they are oscillatory inside the core and formations of superposed waves arise there. This phenomenon of so-called trapped waves has been investigated especially for the core of subsonic jets. For isothermal jets, Towne *et al.* (2017) suggest using a cylindrical vortex sheet on which upstream and downstream propagating acoustic waves are reflected at the shear layers, leading to resonance inside the core. These findings were verified by Schmidt *et al.* (2017) by means of a large-eddy simulation of a Mach 0.9 jet, revealing that these modes are discrete and closely coupled to the instabilities. However, for supersonic jets, the picture is incomplete. Downstream traveling coherent structures are known to play an important role in the process of sound generation (Jordan & Colonius 2013), but a more complete understanding of these structures is lacking. This is one aim of our work.

We focus on purely linear neutral modes supersonic with respect to the outer flow, which link the discrete spectrum with the continuous spectrum. The aim is to investigate linear fundamental mechanisms of sound radiation. In contrast to the method of matched asymptotic expansion, where an outer solution is needed to describe the field-field radiation, the solution underlying our work is inherently oscillatory in the field-field of the jet. Using the symmetry of the plane jet, we reduce the analysis to the analysis of a single shear layer, revealing two classes of modes. The first class of field-field radiating modes we discuss emerges as a neutral limit of a fast traveling second mode instability (Jackson & Grosch 1989). It is therefore very closely related to the supersonic Mach wave radiating instabilities. These modes are subsonic with respect to the constant core flow, meaning that they decay exponentially there and do not contribute to a system of waves inside the core. The second class of modes we discuss is called leaking trapped waves, as it represents a system of reflected waves in the core as well as outward transmitted radiating waves. We explore the underlying mechanism by means of a wave scattering consideration. The basis of our analysis derived from work on the hyperbolic tangent shear layer (Criminale *et al.* 2003; Görtz *et al.* 2024a), from which we construct the planar jet. Acoustic waves are given as an analytical power series solution of the linearized Euler equations, taking into account the singularities in the equations. The boundary conditions (BC) determining the modes are given by a requirement for far-field radiating solutions as well as compatibility with the opposite shear layer through the core flow.

We use the analytically computed modes as input data for a DNS of the jet at high Reynolds number. The jet spreads slightly in the transverse direction due to viscosity and thermal conduction. By this procedure, we use viscosity to regularize the critical layer singularity. The DNS verifies the radiating outgoing character of the modes and shows how the system of trapped waves evolves inside the core.

The work is structured as follows: We summarize the analytic EVP in Section 2, present the DNS setup in Section 3 and show the results of both considerations in Section 4.

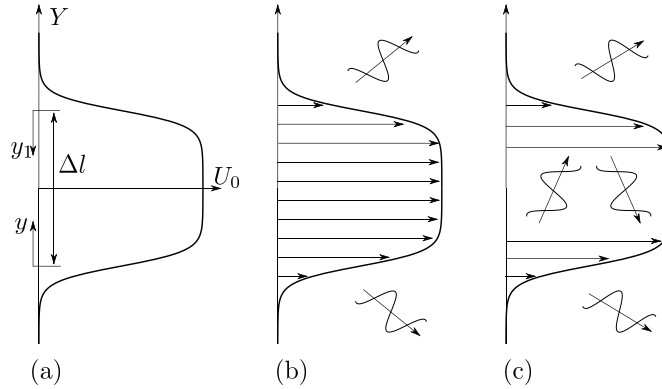


FIGURE 1. (a) Jet flow as superposition of two opposite hyperbolic tangent shear layers (a). Schematic sketches of (b) pure shear layer radiation and (c) leaking trapped wave radiation.

## 2. Modeling and analytical solution

In this section we summarize the analytic derivation of the two classes of eigenmodes.

### 2.1. Model of a plane jet from two shear layers

We are considering a simplified model problem for an isothermal parallel-plane jet superposed by two opposite hyperbolic tangent shear layers, whose mean velocity profile (Figure 1(a)) given by

$$U_0 = \begin{cases} 1/2(1 + \tanh(y_1)) & \text{if } Y > 0, \\ 1/2(1 + \tanh(y)) & \text{if } Y < 0. \end{cases} \quad (2.1)$$

Note that the distance  $\Delta l$  between the two inflection points of the shear layers defined in Figure 1(a) is assumed to be large in comparison to the shear layer thickness, ensuring a good matching of both profiles in Eq. (2.1). Accounting for effects such as non-parallelism is beyond the scope of the mathematical formulation of the analytics made in this work. However, we aim to investigate the basic phenomena from this work for a more complete physical model by means of the DNS. From the symmetry of the main flow velocity profile with respect to the middle of the jet, we reduce all considerations to the lower half of the jet specified by the coordinate  $y$ . Accordingly, BCs are given in the lower field-field as well as by compatibility with the upper half.

Starting with the linearized Euler equations and assuming normal mode perturbations, the amplitude of the acoustic pressure perturbations is described by the compressible Rayleigh equation, which, under the assumption of an isothermal base flow, simplifies to (Criminale *et al.* 2003)

$$\hat{p}''(y) + \frac{2\alpha}{\omega - \alpha U_0(y)} \frac{dU_0}{dy} \hat{p}'(y) + [M^2(\omega - \alpha U_0(y))^2 - \alpha^2] \hat{p}(y) = 0. \quad (2.2)$$

Here,  $M$  is the Mach number,  $\omega$  denotes the temporal frequency, and  $\alpha$  is the wavenumber. We nondimensionalize with the pressure, density, and velocity in the core, whereby we choose as reference length scale the thickness of a single shear layer. For the region of constant mean velocity (i.e., for the free stream and the core of the jet), the asymptotic

solution of Eq. (2.2) is given by

$$\hat{p}(y \rightarrow -\infty) = C_{1/2} e^{\pm i \sqrt{M^2 \omega^2 - \alpha^2} y}, \quad (2.3a)$$

$$\hat{p}(y \rightarrow y_m) = D_{1/2} e^{\pm i \sqrt{M^2 (\omega - \alpha)^2 - \alpha^2} y}, \quad (2.3b)$$

with the middle of the jet given by  $y_m = \Delta l/2$ . For the sake of brevity, the following considerations are carried out for supersonic jets with  $M > 2$ . A more detailed classification of the phase velocity ranges, including  $M < 2$ , is presented by Criminale *et al.* (2003). We aim to analyze neutral modes having a critical layer, that is modes where the phase velocity  $c = \omega/\alpha$  is in the range of the mean flow velocity  $U_0 \in (0, 1)$ . To investigate radiation, we consider modes that are oscillatory in at least the field-field of the jet, which for the lower half is given by  $y \rightarrow -\infty$ . For oscillatory behavior in the field-field, the exponent of the respective asymptotic solution (Eq. (2.3a)) has to be imaginary. This yields neutral modes with supersonic phase velocity with respect to the field-field of the jet, meaning  $1/M < c < 1$ . In that phase velocity range, modes are also supersonic with respect to the constant core flow if  $1/M < c < 1 - 1/M$ , as they are oscillatory in both the constant core flow and the free stream. They therefore lead to a system of trapped waves in the core of the jet, coupling both shear layers. As they radiate outward, they represent the leaking trapped waves. They are conceptually shown in Figure 1(c). The other class of modes that we consider is exponentially behaving in the core and constitutes outgoing waves in the free stream of the jet with a phase velocity range  $1 - 1/M < c < 1$ . We call these modes shear layer radiating modes, as they emerge from each single shear layer. They are sketched in Figure 1(b).

## 2.2. Analytical solution

In order to properly incorporate the BCs, a solution of Eq. (2.2) is needed over the full  $y$  range. Eq. (2.2) together with the hyperbolic tangent main flow profile has four singularities. The solution, following the Fuchs-Frobenius theory (Olver *et al.* 2010), is generally given as a power series around each singularity, converging up to the nearest singularity. Görtz *et al.* (2024a) derive this solution for the hyperbolic tangent velocity profile. According to the BCs specific solution branches of Eqs. (2.3a) - (2.3b) are chosen. The EVP can then be understood as matching the chosen solution branches from the asymptotic solutions in Eq. (2.3) over the whole  $y$  interval by means of the various power series. Below, we discuss the chosen BCs for the two types of modes and introduce the concept of solving the EVP. We start with the BC in the field-field of the jet, which is the same for both types of modes having  $1/M < c < 1$ . We demand outgoing oscillatory solutions in the field-field  $y \rightarrow -\infty$  to describe radiation. These solutions must have negative  $y$ -phase velocity in the limit  $y \rightarrow -\infty$ . According to Eq. (2.3a), the  $y$ -phase velocity of the modes is given by  $\pm \omega / \sqrt{M^2 \omega^2 - \alpha^2}$ . Therefore, in case  $\omega > 0$  we have to choose the constant  $C_1 = 0$ , and if  $\omega < 0$ , then the constant  $C_2 = 0$ . Next, we derive the EVPs for both the pure shear layer radiating and leaking trapped modes by adding BCs in the constant core flow, which are different for the two types of modes.

### 2.2.1. Pure shear layer radiating modes

In the core region  $y \rightarrow y_m$ , we have for the phase velocity range  $1 - 1/M < c < 1$  exponential growth and decay, as the exponent of the asymptotic solution in Eq. (2.3b) becomes real. In order to ensure compatibility with the upper half of the jet, we have to choose the constants as  $D_2 = D_1 e^{-\sqrt{\alpha^2 - M^2 (\omega - \alpha)^2} \Delta l}$ . Using the power series matching

principle described elsewhere (Görtz *et al.* 2024a), we obtain a linear homogeneous  $4 \times 4$  system that ensures matching of the chosen solution branches from Eq. (2.3), now with the constants  $C_2$  and  $D_1$  for  $\omega > 0$  or  $C_1$  and  $D_1$  in case  $\omega < 0$ , which is structurally written as

$$\mathbf{M} \cdot \vec{C} = 0. \quad (2.4)$$

Here, the matrix  $\mathbf{M}$  includes the power series' values at chosen matching points, and  $\vec{C}$  describes the free constants.  $\mathbf{M}$  depends on the Mach number as well as on the eigenvalues  $(\omega, \alpha)$ . Eigenvalues describing pure shear layer radiation are given by  $\det \mathbf{M} = 0$ .

### 2.2.2. Leaking trapped waves

As described above, the second class of modes, having a phase velocity range  $1/M < c < 1 - 1/M$ , is characterized by a system of waves inside the core. Consequently, we have for the lower shear layer both incoming and reflected waves in the core region  $y \rightarrow y_m$ , given by both solution branches in Eq. (2.3b). Unknown at this point are the amplitude ratios between the two waves in the core as well as between the outward radiating wave in the free stream and the incident wave in the core. The solution is obtained by solving the classical wave scattering problem for a single shear layer, which we address elsewhere (Görtz *et al.* 2024b), and which is given by the solution of the inhomogeneous linear  $4 \times 4$  system

$$\tilde{\mathbf{M}} \cdot \vec{r} = \vec{b}, \quad (2.5)$$

where  $\vec{r}$  includes the searched-for amplitude ratios and  $\vec{b}$  contains the incoming wave, which for the jet problem is the one reflected from the opposite shear layer. However, this does not form an EVP since the wave scattering problem for a single shear layer can be solved for arbitrary  $(\omega, \alpha)$ , so an additional condition is needed. This compatibility condition is formed by symmetry and compatibility of the waves in the core with the opposite shear layer. In other words, incoming waves for the lower shear layer are given as reflected waves from the upper shear layer and vice versa. Matching these waves accounts for the role of the distance between the two inflection points  $\Delta l$ , which is closely coupled with the thickness of the constant core flow. This becomes clear since we recognize that for a given thickness of the core flow only specific wavelengths of trapped waves can fit. Because of space constraints, the full derivation of the compatibility condition cannot be shown here. It relates the complex-valued amplitude ratio  $R = D_2/D_1$  between the incident and reflected waves in the core with the inflection point distance  $\Delta l$  and the frequencies of the waves by

$$R = e^{-i\sqrt{M^2(\omega-\alpha)^2-\alpha^2}\Delta l+2i\pi\cdot n}, \quad \text{where} \quad n = 0, 1, \dots, \infty. \quad (2.6)$$

Leaking trapped eigenvalues emerge accordingly for a certain  $\Delta l$  as those values  $(\omega, \alpha)$  where the solution for  $R$ , which is one component of  $\vec{r}$  in Eq. (2.5), fulfills Eq. (2.6). The amplitude ratio between outward radiated waves and the trapped waves is given by  $T = C_1/D_1$  and is included in the solution of Eq. (2.5).

## 3. DNS setup

DNS are carried out using PadeLibs, a high-order computational framework for compressible flows developed at Stanford University (Song *et al.* 2022, 2024). The solver uses sixth-order compact finite-difference methods (Lele 1992; Nagarajan *et al.* 2003;

---

	Mach number	$\Delta l$	$N_x$	$N_y$	$L_x$	$L_y$	$Re$
Case 1	3.062	42	180	768	38.8944	90	30620
Case 2	3.062	77	180	1024	53.8819	142	30620
Case 3	4.2	42	180	832	48.2788	80	42000
Case 4	4.2	77	180	1024	68.949	124	42000

---

TABLE 1. Simulation parameters: number of points  $N_x$  and  $N_y$  and the domain length  $L_x$  and  $L_y$  in  $x$ - and  $y$ -direction, and Reynolds number.

---

Song *et al.* 2022) and a three-stage, third-order, strong-stability-preserving Runge–Kutta (SSPRK3) method for time advancement (Shu & Osher 1988) with CFL = 0.4 to solve the compressible Navier–Stokes equations. Each simulation is run on a two-dimensional uniformly spaced Cartesian mesh based on the analytical eigenfunction for the particular test case. The domain width is specified to be exactly five wavelengths in the  $x$  direction and includes approximately four wavelengths in the free-stream region. The grid is designed to maintain a minimum of 35 points per wavelength in both the  $x$  and  $y$  directions and at least 35 points across the shear layer. The parameters of the four simulations run are shown in Table 1. Each simulation is initialized using flow fields reconstructed from the analytic eigenfunctions. In order to remain in the linear regime, the eigenfunction perturbation amplitude is set to  $10^{-3}$ . The domain is prescribed to be periodic in the  $x$  direction, and a numerical sponge based on the free stream conditions is used to absorb all outgoing waves on the  $\pm y$  boundaries.

A constant viscosity is used across all simulations, which yields Reynolds numbers of  $Re \approx 30,000$  and  $Re \approx 42,000$  based on the shear layer thickness and jet velocity. Gradual jet spreading and heat conduction are expected to produce differences between the analytic base flow and the time-averaged DNS solution. These differences can be reduced by selecting a sufficiently high Reynolds number.

#### 4. Results

We start with a consideration of the analytically computed modes, whose eigenfunctions serve as input for the DNS. We describe them by their  $x$ -phase velocity  $a$  and angle of radiation in the  $x$ – $y$  plane in the field-field, following from Eq. (2.3a) as  $\Phi = \arctan(\alpha/\sqrt{M^2\omega^2 - \alpha^2})$ . Figure 2a shows for both types of modes the angle of radiation plotted over the Mach number, where the color refers to the phase velocity. The solid upper curve represents the pure shear layer radiating modes in the limit  $\Delta l \rightarrow \infty$ , that is for a jet with a very thick core flow. Two main conclusions can be drawn. First, there is one such mode per Mach number, and both the angle of radiation and the phase velocity increase with increasing Mach number. Second, comparing the results with our results on instabilities and resonant over reflection (Görtz *et al.* 2024a,b), we find that the mode emerges as a neutral large-wavenumber limit of the fast second-mode instability of the shear layer, coupling instability with sound radiation and therefore fitting into the picture of Mach wave radiating instabilities.

The second class of modes, representing possible leaking trapped waves, is shown in

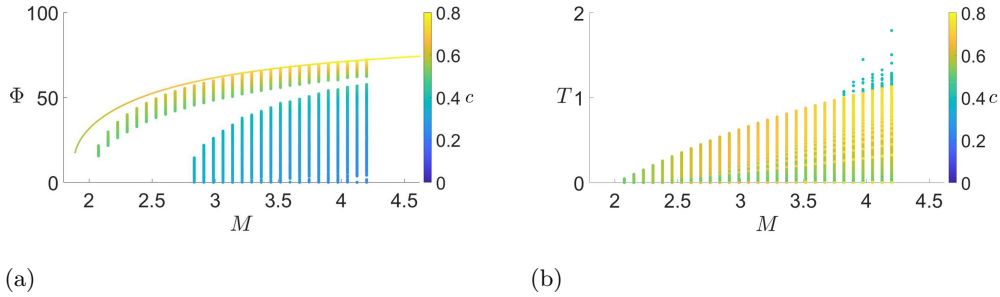


FIGURE 2. (a) Angle of radiation for shear zone radiating modes (solid curve continuous over  $M$ ) and leaking trapped waves (vertical stripes). (b) Absolute value of the radiation coefficient for leaking trapped waves for discrete Mach numbers.

Figure 2a for a discrete set of Mach numbers by the vertical lines. A comment has to be made here regarding the plotted possible modes. From Eq. (2.6), we obtain for the leaking trapped waves both the condition  $|R| = 1$  regarding the absolute value of the amplitude ratio and a condition for the phase of the amplitude ratio, making the occurrence of a specific mode dependent on the inflection point distance  $\Delta l$ . Figure 2a, however, shows all modes with  $|R| = 1$ , whereas for a certain  $\Delta l$ , only several of these modes are picked. We see two regions of possible radiation angles  $\Phi$ , separated by a range of the angle where no radiation occurs for any value of  $\Delta l$ . With increasing Mach number, this range gets smaller. Furthermore, the largest possible angle of leaking trapped waves tends to the angle of the pure shear layer radiating mode as the upper limit.

Another quantity of special interest for the leaking trapped waves is the abovementioned amplitude ratio  $T = C_1/D_1$  between the waves radiated to the field-field and the corresponding trapped waves whose transmission leads to radiation. Figure 2b shows the absolute value  $|T|$  of the amplitude ratio for the possible leaking trapped waves. We observe a significant value in general, increasing with increasing Mach number. For approximately  $M > 3.8$ , we observe  $|T| > 1$ , meaning that certain waves are amplified by the shear layer when transmitted to the field-field. Up to a Mach number  $M \approx 3.8$ , we observe waves with the highest phase velocity being the most amplified ones. For  $M > 3.8$ , an even stronger amplification of waves with low phase velocities occurs, which should be explored in future work.

Below, we discuss the results from the DNS of leaking trapped waves. Figure 3 shows the results for case 1 and 3. The initial condition prescribed by the analytic eigenfunction is compared to the solution after 40 and 100 oscillation periods. The DNS solutions for both test cases appear qualitatively very similar to the initial condition after 40 periods. The trapped waves persist inside the jet, and acoustic waves are leaked to the field-field with similar wavenumbers as the analytic eigenfunctions. For case 1, there is slight growth of the trapped mode by 100 periods, but the shape of the eigenfunction is well preserved. For case 3, there is small distortion of the eigenfunction by 100 periods but no observable growth. For both cases, we observe an increase in the domain-averaged pressure compared with the initial condition. Testing has shown that this growth in the average pressure decreases as the Reynolds number increases and is present even when the initial perturbation amplitude is set to zero. This finding suggests that we are observing a correction to the pressure due to physics not accounted for in the analytic analysis, such as jet spreading and heat conduction. Figure 4 depicts the evolution of the

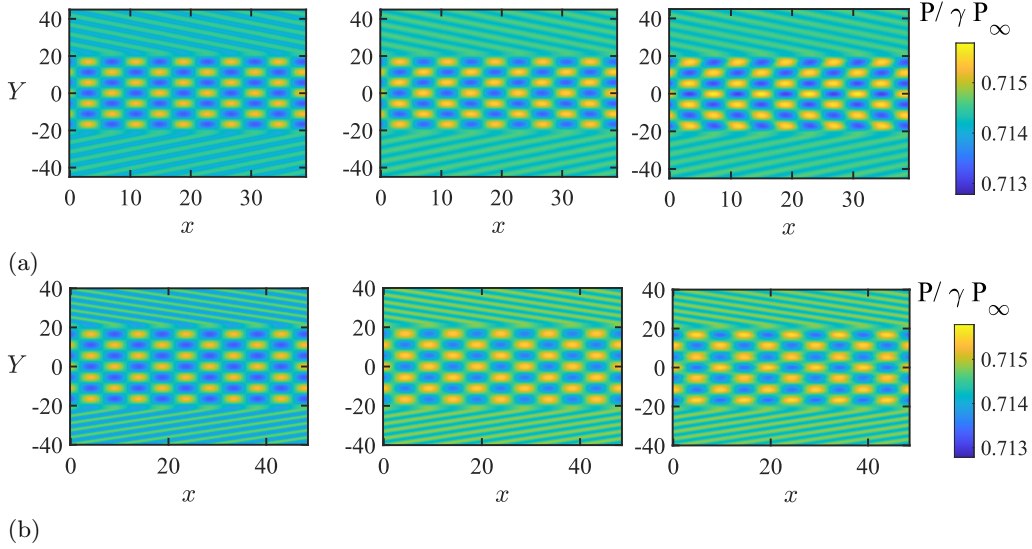


FIGURE 3. Instantaneous pressure for (a) case 1 with  $M = 3.06$ ,  $\Delta l = 42$  and (b) case 3 with  $M = 4.2$ ,  $\Delta l = 42$ . Fields are plotted from left to right at  $t/T = 0$  (initial condition),  $t/T = 40$ , and  $t/T = 100$ , where  $T = 2\pi/\omega$  is the analytic oscillation period.

eigenfunction shape more quantitatively for all four test cases. The numerical solution is plotted as a function of the transverse coordinate at an  $x$  location of maximum centerline pressure after several oscillation periods. As shown in Figure 3, the increase in domain-averaged pressure with time causes the center of oscillation in Figure 4 to move to higher pressure. Figure 5 plots the maximum pressure disturbance amplitude—found by subtracting the instantaneous domain-averaged pressure from the instantaneous pressure field—is plotted as a function of time in both the jet core and the free-stream. For all test cases, well-defined core and free-stream modes persist with wavenumbers that match the analytic results very well for 100 oscillation periods. For test cases 1–3, the amplitudes of the trapped and free stream modes remain relatively constant in time. For case 4, however, there was non negligible growth and distortion of the trapped mode with time. Therefore, a second simulation for case 4 was run with increased grid resolution in both  $x$  and  $y$  directions ( $N_x = 250$ ,  $N_y = 1434$ ). The amplitudes for this test case are plotted with a green line in Figure 5, and the shape of the trapped mode after 100 periods is shown in Figure 4(d). Refining the grid helps to both preserve the shape of the trapped mode and reduce the growth rate, suggesting that the primary differences between the analytic eigenfunction and the DNS results are due to numerical errors accumulating over time. Further refinement of the grids for cases 1–3 may be expected to similarly improve agreement with the prescribed initial conditions.

## 5. Conclusions

In this work, we studied continuous modes with far-field radiating character in a parallel plane supersonic jet with constant core flow. We gave an inviscid treatment of the problem, revealing the modes as solutions of two EVPs. By means of a DNS, we verified the far-field radiating character and the system of waves inside the core flow of the jet for the found leaky trapped waves. A major goal of our work was to establish a link

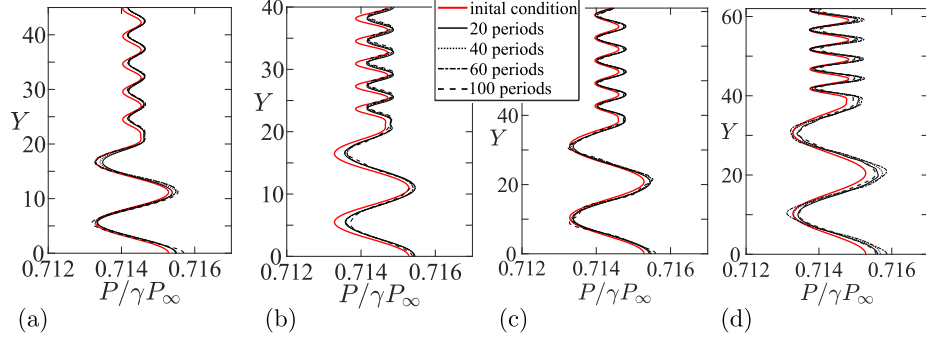


FIGURE 4. Pressure fluctuations after several oscillation periods compared with the analytic eigenfunctions. (a–d): cases (1–4). For case 4, the result after 100 periods is given on the refined grid ( $N_x = 250, N_y = 1434$ ).

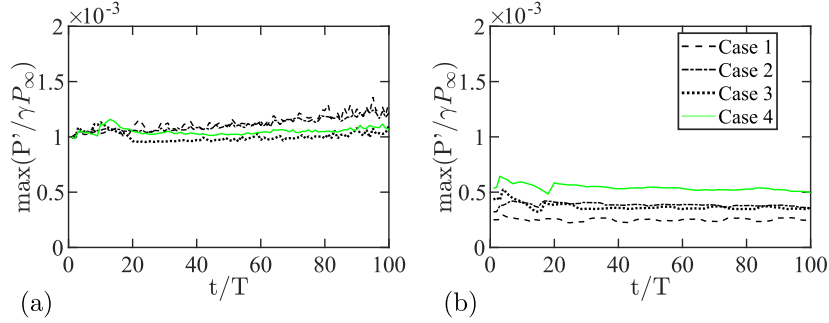


FIGURE 5. Maximum pressure perturbation in (a) the jet core and (b) the free stream. The disturbance amplitude for case 4 on a refined grid ( $N_x = 250, N_y = 1434$ ) is plotted in green.

between the discrete- and continuous-mode spectra in a jet to clarify how continuous neutral modes, which allow far-field radiation directly without any matching, can be related to the concept of Mach wave radiation due to instabilities. This was done because continuous far-field radiating neutral modes have been found to be the limits of Mach wave radiating instabilities. Such modes are generated separately in both shear zones and have exponential character toward the centerline of the jet. The second class of radiating modes, however, closely couples both shear layers through a system of trapped waves in the core flow, contributing to the question of large downstream traveling structures in the core of a jet and their role in noise emission. The existence of these modes has been confirmed by DNS. Several extensions of the current work are conceivable. Whether a more complete physical model of a non-parallel evolving jet confirms the same types of radiating modes should be investigated. And more challenging, a change to unstable modes with randomized phases as initial conditions should be considered to investigate whether a time-evolving jet will later exhibit the modes found in this work.

#### Acknowledgments

The authors are very grateful to Hang Song for his extraordinary support with the DNS and to Peter Schmid for helpful discussions on noise generation and instabilities in jets.

## REFERENCES

- CRIMINALE, W. O., JACKSON, T. L. & JOSLIN, R. D. 2003 *Theory and Computation of Hydrodynamic Stability*. Cambridge University Press.
- GÖRTZ, S., DE BROECK, L., HOLLMANN, P., ALTER, P. & OBERLACK, M. 2024a Theory of acoustics in compressible shear layers. part 1. instability induced radiating modes. *under review with the J. Fluid Mech.* .
- GÖRTZ, S., DE BROECK, L., HOLLMANN, P. & OBERLACK, M. 2024b Theory of acoustics in compressible shear layers. part 2. wave scattering, resonant over reflection and instability inducing wave absorption. *under review with the J. Fluid Mech.* .
- JACKSON, T. L. & GROSCH, C. E. 1989 Inviscid spatial stability of a compressible mixing layer. *J. Fluid Mech.* **208**, 609–637.
- JORDAN, P. & COLONIUS, T. 2013 Wave packets and turbulent jet noise. *Annu. Rev. Fluid Mech.* **45** (Volume 45, 2013), 173–195.
- LELE, S. K. 1992 Compact finite difference schemes with spectral-like resolution. *J. Comput. Phys.* **103**, 16–42.
- LIGHTHILL, M. J. 1952 On sound generated aerodynamically. I. General theory. *P. R. Soc. A* **211**, 564–587.
- MITCHELL, B. E., LELE, S. K. & MOIN, P. 1997 Direct computation of Mach wave radiation in an axisymmetric supersonic jet. *AIAA J.* **35**, 1574–1580.
- NAGARAJAN, S., LELE, S. K. & FERZIGER, J. H. 2003 A robust high-order compact method for large eddy simulation. *J. Comput. Phys.* **191**, 392–419.
- OLVER, F. W. J., LOZIER, D. W., BOISVERT, R. F. & CLARK, C. W. 2010 *The NIST Handbook of Mathematical Functions*. Cambridge Univ. Press.
- SCHMIDT, O. T., TOWNE, A., COLONIUS, T., CAVALIERI, A. V. G., JORDAN, P. & BRÈS, G. A. 2017 Wavepackets and trapped acoustic modes in a turbulent jet: coherent structure eduction and global stability. *J. Fluid Mech.* **825**, 1153–1181.
- SHU, C.-W. & OSHER, S. 1988 Efficient implementation of essentially non-oscillatory shock-capturing schemes. *J. Comput. Phys.* **77**, 439–471.
- SONG, H., GHATE, A. S., MATSUNO, K., WEST, J., SUBRAMANIAM, A., BROWN, L. J. & LELE, S. K. 2022 Robust high-resolution simulations of compressible turbulent flows without filtering. In *AIAA Paper # 2022-4122*.
- SONG, H., GHATE, A. S., MATSUNO, K. V., WEST, J. R., SUBRAMANIAM, A. & LELE, S. K. 2024 A robust compact finite difference framework for simulations of compressible turbulent flows. *J. Comput. Phys.* **519**, 113419.
- TAM, C. K. 1995 Supersonic jet noise. *Annu. Rev. Fluid Mech.* **27**, 17–43.
- TAM, C. K. W. 1971 Directional acoustic radiation from a supersonic jet generated by shear layer instability. *J. Fluid Mech.* **46**, 757–768.
- TAM, C. K. W. & BURTON, D. E. 1984 Sound generated by instability waves of supersonic flows. Part 1. Two-dimensional mixing layers. *J. Fluid Mech.* **138**, 249–271.
- TAM, C. K. W. & HU, F. Q. 1989 On the three families of instability waves of high-speed jets. *J. Fluid Mech.* **201**, 447–483.
- TOWNE, A., CAVALIERI, A. V. G., JORDAN, P., COLONIUS, T., SCHMIDT, O., JAUNET, V. & BRÈS, G. A. 2017 Acoustic resonance in the potential core of subsonic jets. *J. Fluid Mech.* **825**, 1113–1152.
- WU, X. & ZHANG, Z. 2019 First-principle description of acoustic radiation of shear flows. *T. R. Soc. A* **377**, 20190077.